ACS OMEGA

http://pubs.acs.org/journal/acsodf

Article

Synthesis, Characterization, and Performance of Pyridomethene−BF2 Fluorescence Dye-Doped PVA Thin Film and PVP Nanofibers as Low γ-ray Dosimeters

Sadeq M. Al-Hazmy,* Yassine EL-Ghoul,* Jameelah Al-Harby, Haja Tar, and Fahad M. Alminderej*

Cite This: *ACS Omega* 2022, 7, 34002−34011

Read Online

ACCESS | Metrics & More | Article Recommendations

ABSTRACT: Currently, particular attention is paid to public health related to the field of γ-ray dosimetry, which is becoming increasingly important in medical diagnostic processes. Incorporating sensitive dyes as radiation dose sensors in different material hosts has shown promising radiation dosimetry application routes. In this perspective, the current study proposes a new fluorescent dye based on boron difluoride complex, the pyridomethene−BF2 named 2-(1-(difluoroboraneyl)-1,2-dihydroquinolin-2-yl)-2-(1-methylquinoxalin-2-ylidene) acetonitrile (DBDMA) as an indicator for low γ-ray doses. The different optical and quantum chemical parameters and the spectral behavior of the selected fluorescent dye were first studied. Then, PVP/DBDMA electrospun nanofibers and PVA/DBDMA thin films were prepared. The different UV−vis spectrophotometric and fluorescence studies revealed a clear change after exposure to different γ-ray doses. Thermogravimetric analysis exhibited excellent thermal stability of the prepared nanocomposite films, showing altered thermal behavior after γ-ray treatment. Furthermore, the SEM evaluation displayed a significant modification in the surface morphology of the two designed nanomaterials with increased radiation dose intensity. These novel forms of dosimeter designed in nanoscale composites could therefore constitute a promising and efficient alternative for rapid and accurate detection of low doses of γ-rays in various medical applications.

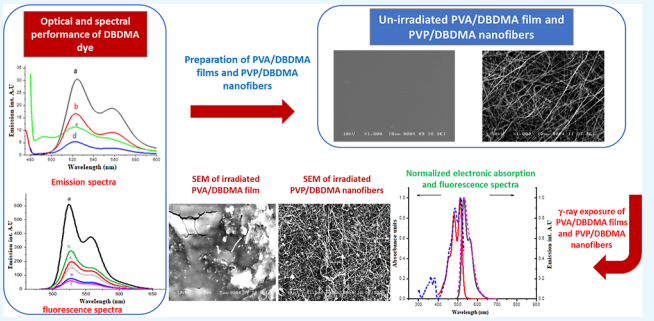

1. INTRODUCTION

Radiation treatment is a technique widely explored in several fields, including polymerization, sterilization of surgical devices, food irradiation, and diagnostic radiology.[1−5] Depending on the area of investigation, different level doses are selected carrying a high, medium, or low intensity.

The detection or accurate quantification of the radiation dose delivered has become a necessity and a significant challenge in various applications. In particular low radiation doses constitute a real problem today due to the non-availability of suitable dosimeters in this range.[6,7] Several forms of dosimeters suitable for various dose intensities have been studied and have made rapid progress, such as photographic films and Geiger−Muller and proportional counter.[8,9] Standard solutions having the properties of color or oxidation state changes have been widely studied.[10,11] However, the complexity of handling the solution, the recording time, and the need for heavy and expensive auxiliary instrumentation for dose detection such as UV−vis, electron spin resonance, NMR, infrared (IR), and thermoluminescence have intensified the need to find more effective alternatives.[12,13] Nowadays, it is beneficial to have practical and easy-to-explore dosimeters offering a direct reading of doses without recourse to the auxiliary instruments. The most obvious solution was to exploit the physical, optical, and color changes following radiation treatment.[14,15] The most widespread solution was based on composite films whose matrix is an easy-to-cast polymer that interacts with different host molecules without affecting their colorimetric, physical, or optical characteristics.[16,17] At present, functional polymers are widely investigated in various fields.[18−22] Several polymers have been reported as matrices of thin-film dosimeters, such as PVA, nylon-6, polystyrene, polymethyl methacrylate, and polyvinyl chloride. Their possible doping using different dyes preceding their irradiation was studied, and their dosimetric efficiency was evaluated.[23−25] In line with this, the investigation of PVA-doped films has shown great interest in several studies and research.[26,27] PVA has shown more opportunities due to its low cost, availability, nontoxicity, water solubility, and ability to incorporate a wide

Received: May 21, 2022
Accepted: August 9, 2022
Published: September 15, 2022

range of transition metal salts and dyes.[28−30] Currently, nanofibrous materials via different electrospinning technologies are widely reported and proven effective in various biomedical applications including tissue engineering, wound dressing, drug delivery, regenerative medicine, disease modeling, and detection/biodetection.[30−33] These sustainable electrospun composites were effective due to their ease of operation, nanoscale diameter, wide specific surface, high porosity, cost-effectiveness, and the considerable adaptability for engineering eco-friendly bioactive nanomaterials.[34,35] Electrospun nanomaterials synthesized by mixing high molecular weight polymers and different sensitive dye molecules could be an effective way to prepare various nanomaterials as dosimeters of different γ-ray exposure levels.

The current study aims to take part in the excellent colorimetric, optical potential, and spectral behavior of pyridomethene−BF2 complex (DBDMA) to synthesize γ-ray nanocomposite dosimeters in different matrix hosts. The first is a film-based PVA polymer-doped DBDMA and the second is a DBDMA incorporating electrospun PVP nanofibers. Different parameters of film casting and nanofiber preparation are first optimized. The two nanocomposite materials were then exposed to various γ-radiation doses. After irradiation treatment, the various chemical, structural, physical, and morphological changes were evaluated via FTIR, UV, thermogravimetric analysis (TGA), and SEM analyses. Moreover, the different response behaviors, revealed by these characterizations, as a function of increasing γ-ray doses applied to the two nanocomposite hosts were studied in order to evaluate their dosimetric performances for the routine γ-irradiation process.

2. MATERIALS AND EXPERIMENTAL METHODS

2.1. Materials. The dye used in the present study is 2-(1-(difluoroboraneyl)-1,2-dihydroquinolin-2-yl)-2-(1-methylquinoxalin-2-ylidene) acetonitrile (DBDMA). It is kindly offered by Professor Ewald Daltrozzo of the Faculty of Chemistry at the University of Konstanz in Germany. It is also synthesized and characterized by Kubota et al.[36] PVA polymer (M_w: 89 000−98 000, 99%, with a hydrolysis degree of 85−90%) and PVP (M_w: 1.300.000, 99.9%) were purchased from Sigma-Aldrich (St. Louis, USA). Ultrapure water (Milli-Q Direct, Darmstadt, Germany) was used to prepare different films and electrospun nanomaterials. All reagents were of analytical grade and were used without further purification.

2.2. Characterization. The synthesized nanofiber materials and nanocomposite films were characterized via various techniques. The responses of raw and irradiated nanomaterials at different doses were compared to assess their effectiveness as low γ-ray dosimeters.

FTIR characterization using the attenuated total reflection mode was carried out to obtain IR spectra of raw and irradiated nanomaterials. An IR spectrophotometer (Agilent Technologies/Gladi-ATR, Santa Clara, CA, USA) was used in a fixed range varied from 4000 to 400 cm^{-1}. A resolution of 4 cm^{-1} was set to measure different IR spectra.

A UV−vis spectrophotometer (Shimadzu, UV-2501PC, Kyoto, Japan) was explored to determine the absorption curves of the different nanomaterial labels. The measurements were applied on a wavelength scale varying from 200 to 700 nm. Steady-state measurements of the DBDMA dye and the different prepared nanomaterials were carried out using a JASCO FP-8200 spectrometer (JASCO, Riyadh, Saudi Arabia), with an excitation bandwidth of 5 nm and an emission bandwidth of 5 nm, using a Xe lamp light source.

Photochemical quantum yields of DBDMA (φc) were measured using a modified A. J. Lees's method considering the decrease in absorbance at the excitation wavelength as photo-irradiation proceeds.[37]

2.2.1. Fluorescence Quantum Yields. Fluorescence quantum yields in liquid were determined using the optically dilute solution relative method with either 9,10-diphenyl-anthracene or quinine sulfate solutions, depending on the emission wavelength range. The intensity of light was determined using ferrioxalate actinometry.[38,39] The following eq 1 was applied to calculate the fluorescence quantum yields.

$$\varnothing_f(s) = \varnothing_f(r) \times \frac{\int I_s}{\int I_r} \times \frac{A_r}{A_s} \times \frac{n_s^2}{n_r^2} \quad (1)$$

The integrals denote the corrected fluorescence peak areas, "*A*" represents the absorbance at the excitation wavelength, and "*n*" denotes the solvent's refractive index. The subscripts "s" and "r" indicate that this is a sample and a reference.

Thermal stability and different thermal characteristics of prepared thin-film nanocomposites were evaluated via thermogravimetric measurements using a TA Instruments apparatus. The fixed parameters for different TGA analyses were a heating rate of 10 °C min^{-1} and a temperature range from 25 to 600 °C.

SEM analysis was performed on raw and irradiated nanocomposite films and electrospun nanofibers to evaluate their morphological behavior after varied X-ray doses. SEM micrographs were accomplished via SEM (JEOL JSM-5400 LV, JEOL Ltd., Akishima, Japan). The measurements were carried out under an acceleration voltage of 5 kV. Magnifications ranged from 100 to 2000×. To improve the surface conductivity of the tested samples, a surface coating of a thin layer of Au was applied before the analysis.

2.3. Preparation of PVA/DBDMA Nanocomposite Films. The film-based PVA polymer mixed with various amounts of DBDMA filler was developed following a previously reported casting method in our laboratory.[40] A 5% solution of PVA dissolved in distilled water was prepared. The bulk solution was then heated gently using a controlled temperature with a heater instrument. The preparation was kept under continuous stirring at a constant temperature of 80 °C. After 2 h, the polymer solution was cooled to an ambient temperature, and DBDMA solution (0.04% dissolved in 10 mL of ethanol) was poured into the clear, viscous solution of PVA. After 1 h of stirring without heating, 20 mL of the solution was poured into glass Petri dishes. The dishes were then set to dry in the dark (to avoid direct exposure to light) at room temperature for 3 days. The thickness of peeled films was then measured using a numerical thickness instrument. The mean value of the thickness of films was around 100 μm. The nanocomposite films were finally cut into small pieces of 2 cm sides and stored in black envelopes away from any light to avoid their possible deterioration and achieve thermal equilibrium before their subsequent use.

2.4. Preparation of PVP/DBDMA Nanofiber Material. The formation of DBDMA-doped PVP nanofiber begins. When a critical potential is reached, the jet solution is expelled from the Taylor cone and deposited on the collector. A prepared solution of PVP polymer (2×10^{-3} M) doped with DBDMA (1.2×10^{-6} M) was subjected to nanofiber

https://doi.org/10.1021/acsomega.2c03174
ACS Omega 2022, 7, 34002−34011

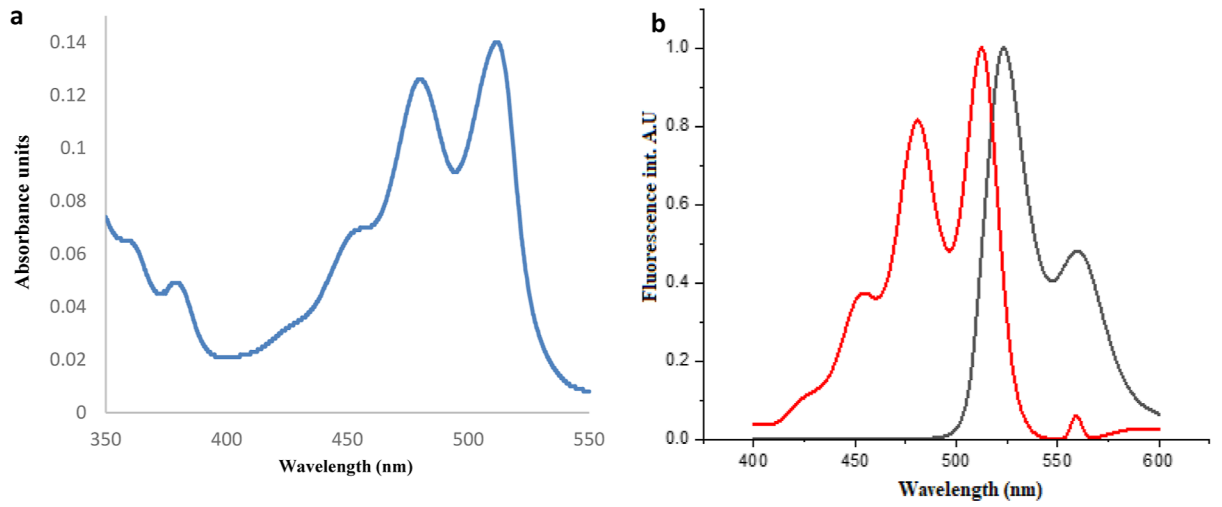

Figure 1. Absorption spectra of 2.9×10^{-6} M DBDMA in chloroform (a) and normalized red emdash absorption and black emdash fluorescence spectra of 2.8×10^{-7} mol dm^{-3} in chloroform, λ_{ex} = 512 nm (b).

fabrication using *aY*-flow Professional lab device Nano-technology electrospinning machine. The electrospinning procedure was conducted at a voltage of 30 kV. A distance of 17 cm was set between the stationary collection plate and the tip of the blunt syringe needle. The flow rate was set at 5 L/min. The generated nanomaterial was collected on an aluminum foil placed over the fixed collecting plate.

3. RESULTS AND DISCUSSION

3.1. Effect of Media on the Spectral Characteristics of the DBDMA Dye. The absorption spectrum of DBDMA in chloroform shows narrow absorption bands with three absorption maxima similar in shape to boron dipyrromethene dye.[41] The 0−0 band of a strong S_0−S_1 transition with a maximum appearing at 511 ± 3 nm. At the short wavelength, the second maximum is centered at about 475 and 451 nm and attributed to the same transition's 0−*n* vibrational band. In addition, the S_0−S_2 transition is characterized by relatively low absorption value bands at around 379 nm, as shown in Figure 1a.

The high molar absorptivity of DBDMA and the mirror image relationship between excitation and fluorescence spectra are consistent with a strongly allowed (π−π^*) transition with a small geometry change between electronic ground and excited states as shown in Figure 1b for the studied dyes in chloroform.[38] A slight Stokes shift of 8 nm is observed, indicating a poor excited state. The emission spectrum shows vibrational structure due to a lack of ground-state solvation, as shown in Figure 1b.

3.2. Effect of Acidity on Absorption and Emission Spectra. Methyl sulfonic acid (MSA) is a strong organic acid. Its addition leads to the protonation of nitrogen heteroatoms, transforming it from an electron-donating center into an electron-withdrawing center. It is well known that electron-donating centers cause fluorescence enhancement, whereas electron-withdrawing centers reduce fluorescence efficiency. This explains the decrease in fluorescence intensities upon increasing the MSA concentration. Unlike fluorescence, absorbance is less affected by protonation. Figures 2 and 3 show a robust regular reduction in fluorescence of DBDMA by the addition of MSA due to protonation. This excludes the possibility of pH tuning for DBDMA as a laser dye.[42−44]

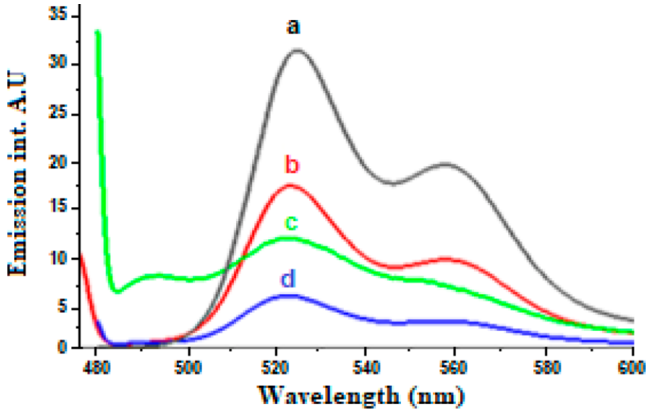

Figure 2. Emission spectra of 2.2×10^{-5} mol dm^{-3} DBDMA in ethanol shows a decrease in emission intensity at increasing concentrations of sulfonic methyl acid (a) 0.0, (b) 2.1×10^{-4}, (c) 2.6×10^{-4}, and (d) 3.5×10^{-4} M. λ_{ex} = 514 nm.

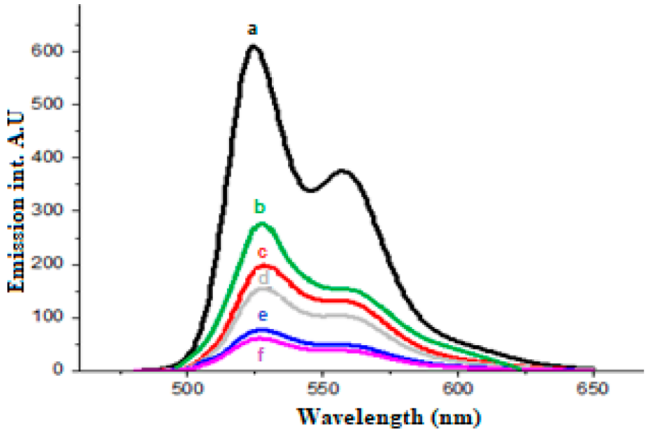

Figure 3. Fluorescence spectra of 1.4×10^{-5} M DBDMA in CH3CN at different $[H_0]$ values. The values of H_0 at decreasing emission intensities: (a) 0.0, (b) 0.18, (c) 0.37, (d) 0.74, (e) 1.1, and (f) 1.8 A.U.

A corresponding decrease in the absorbance is observed upon the addition of MSA to 7.6×10^{-6} M DBDMA in acetonitrile solution, as shown in Figure 4. This is related to

https://doi.org/10.1021/acsomega.2c03174
ACS Omega 2022, 7, 34002−34011

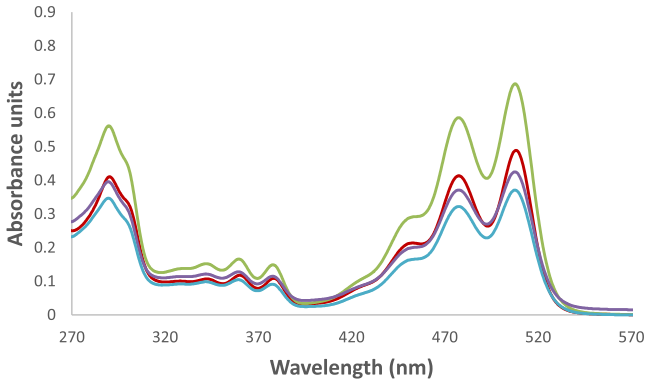

Figure 4. Electronic absorption spectra of 7.6×10^{-6} M DBDMA in acetonitrile decreasing absorbance at increasing % of MSA, green emdash 0.0%, red emdash 0.006%, voilet emdash 0.007% and blue emdash 0.009%.

the molecule's allowedness and forbiddenness of electronic transitions because of its protonation. No extra bands were detected under prevailing experimental conditions.

According to the half-height method, the protonation constant of the ground state (pK_a) was determined using fluorometric titration, as shown in Figure 5. The value of pK_a was determined as 0.56 from emission spectra.[45,46]

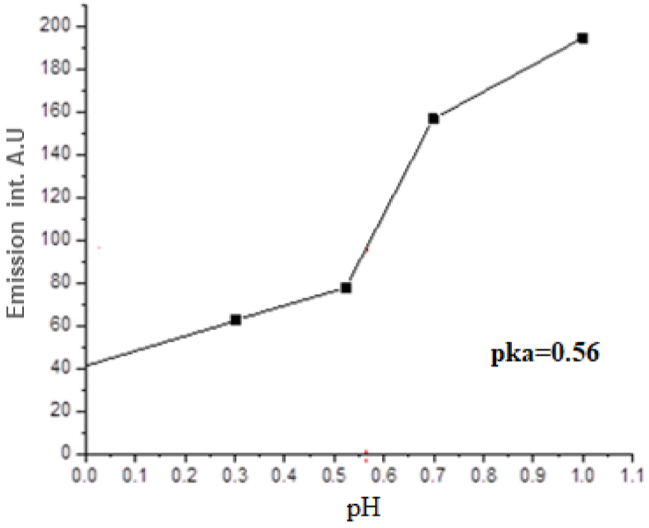

Figure 5. lot of emission intensities of 1.4×10^{-5} mol dm^{-3} DBDMA at λ_{em} = 528 nm against pH values.

3.3. Photostability of DBDMA. The photochemical quantum yield (ϕ_c) values (~0.003±) of DBDMA in chloroform, thin-film, and nanofiber are summarized in Table 1. The low values of ϕ_c indicate photostability against irradiations. Figure 6 shows no change in emission intensity of the studied dye upon irradiation using 365 nm for 24 h

Table 1. Fluorescence Quantum Yield (Φ_f) and Photochemical Quantum Yield (ϕ_c) in Chloroform

solvent	$\lambda_{em\ max}$ (nm)	$\lambda_{abs\ max}$ (nm)	Φ_f λ_{abs} max	Φ_c
$CHCl_3$	532	512	0.70	0.003
DBDMA-doped PVP	528	520	0.3	-
DBDMA-doped PVA	533	512	0.1	0.004

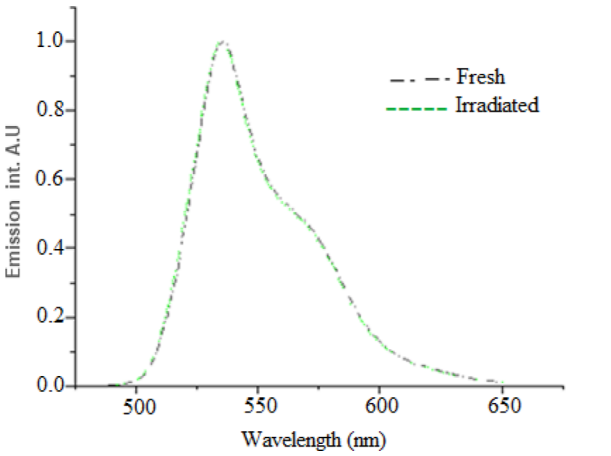

Figure 6. Fluorescence spectra of fresh and irradiated 1.4×10^{-6} mol dm^{-3} DBDMA solution in ethanol. Irradiation wavelength is 365 nm for 24 h.

which is attributed to the rigidity of the molecules, which has also been confirmed by the slight shift in the emission and absorption wavelengths as the solvent's polarities change. The rigidity of the molecule is approved by the high fluorescence quantum yield. This high fluorescence quantum yield indicates that reabsorption is avoided. The remarkable DBDMA dye photostability and its high fluorescence quantum yield (Φ_f) values allow its potential application in many areas, including dye lasers and solar cell collectors.[47,48]

3.4. Spectral Characteristics of Dye-Doped PVP Nanofiber and Dye-Doped PVA Films. DBDMA in solid hosts, including electrospun nanofibers and PVA thin films, showed structured and peak-shifted emission compared to the emission obtained for $CHCl_3$ solution. The structured criterion of the spectra is attributed to the restriction of the rotational mode of molecular motion in solid matrices due to the condensed phase cage effect.[49]

A slight Stokes shift of 8 nm, a perfect coincidence between absorption and excitation spectra, maximum wavelengths, and the full width at half-maximum are observed between DMF solution and nanofiber structure as shown in Figure 7. DBDMA-doped PVP nanofiber prepared from 1.2×10^{-6} mol dm^{-3} shows an absorption peak at 52 nm and an apparent fluorescence emission with a structured band peak at 528 nm using λ_{ex} = 450 nm, as shown in Figure 8. Low concentrations were used to avoid reabsorption. This makes DBDMA-doped PVP of a promising application in electronic devices. All these similar properties between absorption and fluorescence spectra of DBDMA in both DMF solution and dye-doped PVP nanofiber suggest the formation of neither aggregation in the ground state nor an excimer in the excited state. As the difference between the emission spectra of the same dye-doped PVP and that in the ethanol solvent shows, a simple blue shift of 9 nm with the appearance of resolved Franck−Condon fluorescence peak at 556 nm is observed in Figure 9. A slight change in the excitation spectrum is observed. The wavelength of the band peaks was shifted by only 2 nm going with the dye from an ethanol solution to dye-doped PVP nanofibers, as shown in Figure 10.

The emission spectrum of dye-doped PVA thin film has a remarkable decrease in the fluorescence quantum yield compared to its peers in various media previously explained as given in Table 1. The normalized fluorescence spectra of

https://doi.org/10.1021/acsomega.2c03174
ACS Omega 2022, 7, 34002−34011

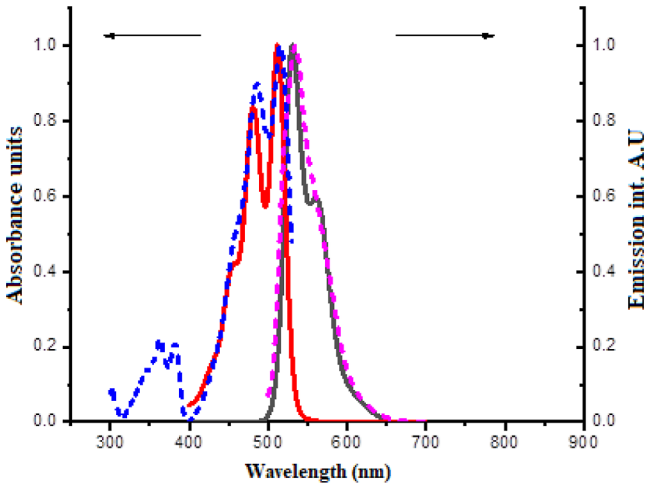

Figure 7. Normalized electronic red emdash absorption and black emdash fluorescence spectra of DBDMA in DMF solution, and blue hyphen absorption and pink hyphen fluorescence spectra of DBDMA-doped PVP nanofiber, λ_{ex} = 488 nm.

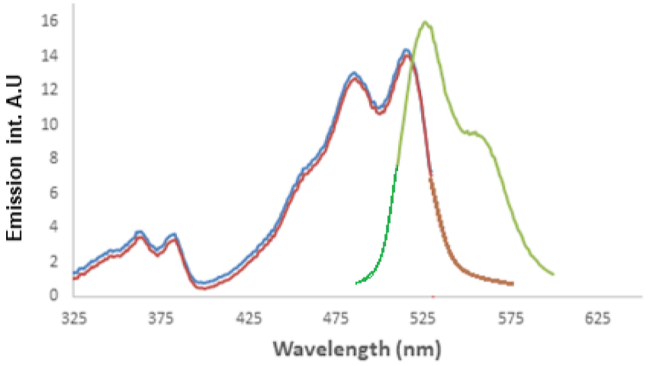

Figure 8. Absorption brown emdash, fluorescence green emdash spectra, λ_{ex} = 488 nm and excitation black emdash spectra, λ_{emmax} = 540 nm of DBDMA-doped PVP nanofibers.

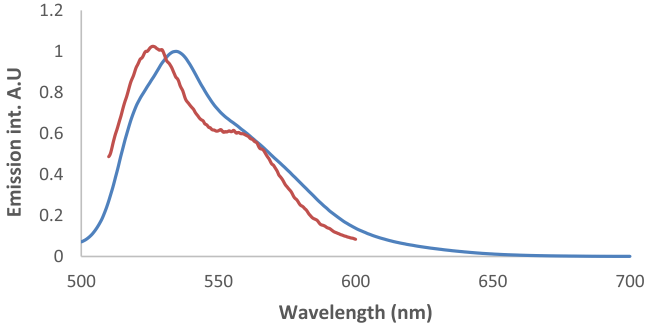

Figure 9. Normalized fluorescence spectra of orange emdash DBDMA-doped PVP nanofibers prepared from ethanol solution and blue emdash 2.9 × 10^{-6} M DBDMA in ethanol, λ_{ex} 500 nm.

DBDMA-doped PVP nanofiber and DBDMA-doped PVA thin film show an emission band peak at a shorter wavelength of 492 nm for DBDMA-doped PVP with only a shoulder at 551 nm. In contrast, for DBDMA-doped PVA, there is a peak at 551 nm and a disappearance of the peak at 492 nm for and resolved Franck–Condon fluorescence peak at 551 nm, as shown in Figure 11.[50]

3.5. γ-ray Effect on Nanofiber and Thin-Film Composites. *3.5.1. Absorption and Fluorescence Spectra.*

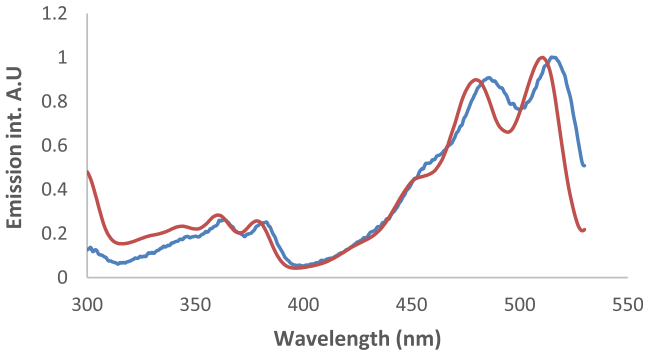

Figure 10. Excitation spectra of DBDMA brown emdash ethanolic solution 2.9 × 10^{-6} M and blue emdash nanofabricated with PVP polymer (4%).

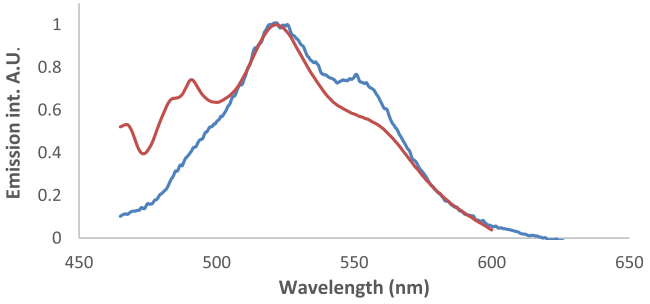

Figure 11. Normalized fluorescence spectra of brown emdash DBDMA-doped PVP nanofiber and blue emdash DBDMA-doped PVA thin film, λ_{ex} = 450 nm.

Irradiation of dye-doped PVP using γ-rays (dose = 420 mR) results in the disappearance of a resolved Franck–Condon fluorescence peak at 561 nm and a blue shift of 4 nm, as shown in Figure 12. However, irradiation of the DBDMA-doped PVA

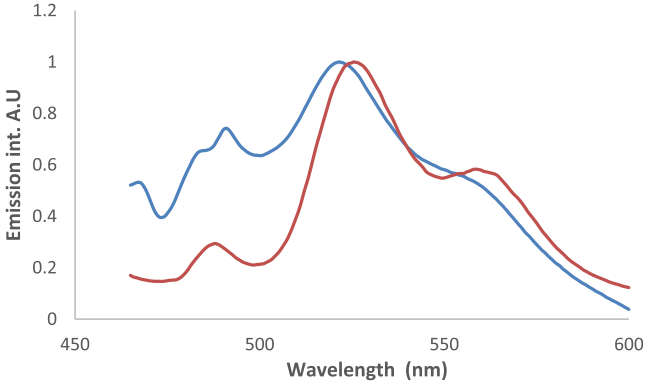

Figure 12. Normalized fluorescence spectra of DBDMA-doped PVP brown emdash fresh and blue emdash irradiated, dose: 220 mR (λ_{ex} = 450 nm).

thin layer using the same rays and duration increased the emission intensity, as shown in Figure 13a. This increase is accompanied by the disappearance of the resolved Franck–Condon peak in addition to a red shift from 522 nm in the fresh sample to 563 nm in the irradiated sample. It may be due to molecular aggregation or excimer formation because of a mutation compound due to irradiation, see Figure 13b (normalized version of Figure 13a). This red shift and disappearance of Franck–Condon peaks were not observed

https://doi.org/10.1021/acsomega.2c03174
ACS Omega 2022, 7, 34002–34011

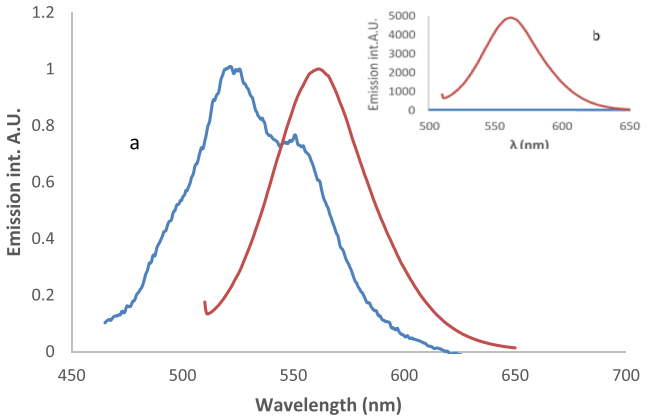

Figure 13. Normalized fluorescence (a) and fluorescence spectra (b) of DBDMA-doped 5% PVA blue emdash fresh and brown emdash irradiated samples (dose = 220 mR), λex = 500 nm.

in the ground state, as there was no change in the absorption spectrum. There was only a decrease in the intensity of the absorbed light without any change in the spectra. The changes in the positions of the emission peaks together with the change in the fluorescence and absorption intensities of DBDMA-doped PVP nanofiber and DBDMA-doped PVA thin film as a result of exposure to very low doses of γ-rays (between 150 and 420 mR) confirm the efficacy of using this dye as a probe to identify the presence of γ-rays as shown in Figure 14.

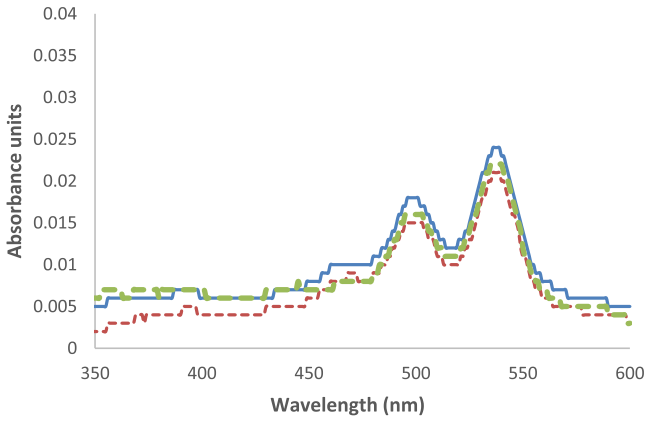

Figure 14. Absorption spectra of DBDMA-doped PVA thin film, blue emdash fresh and irradiated using γ-rays, green hyphen 150 mR and brown hyphen 420 mR.

3.5.2. FTIR analysis. The irradiation of the DBDMA-doped PVP nanofiber induced significant variations in the structure of the sample, as indicated by FTIR spectra as shown in Figure 15. The broad band at 3300−3500 cm^{-1}, ascribed to the stretching modes of overlap of CO−H vibrations, has been shifted to a higher wavenumber after irradiation which implies the peak O−H after irradiation. This finding may be due to the increasing extent of hydrogen bonding or cross-linking. Again, the intensity of the peak C═O stretching (at 1650 cm^{-1}) was increased. C−O (at 1050 cm^{-1}) was increased in the irradiated sample, proving the possibility of interchange between the two groups. This could be due to the occurrence of keto−enol tautomerism and hydride migration between carbon and oxygen within the network of the PVP polymer.[51]

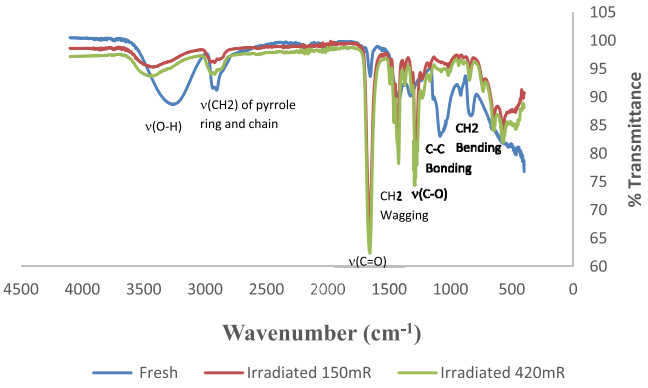

Figure 15. FTIR spectra of DBDMA-doped PVP nanofibers fresh and irradiated with 150 and 420 mR.

The effect of the irradiation on the chemical structure of the thin-film DBDMA-doped PVA is illustrated in Figure 16,

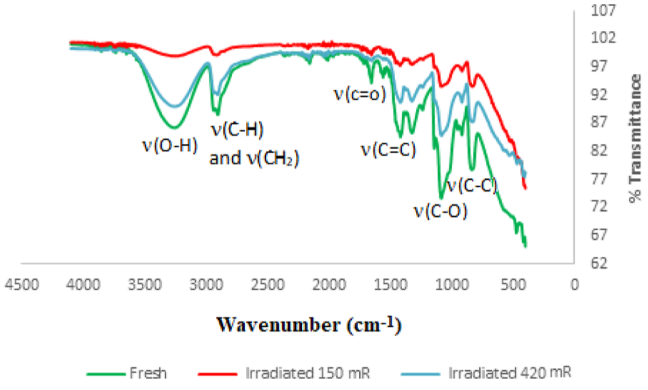

Figure 16. FTIR spectra of DBDMA-doped PVA thin film, fresh, irradiated with 150 and 420 mR.

where the exposed films to different γ-ray doses (150 and 420 mR) are compared with the non-irradiated sample. A decrease in the intensity of the peaks of all functional groups is observed in the irradiated samples. However, the positions of all peaks remained basically in the same positions. Besides, no additional peaks are observed in the irradiated samples. These results indicate that irradiation with low γ-ray doses imposed limited influence on the chemical structure of the thin-film DBDMA-doped PVA sample.

3.5.3. Thermal Analysis of the PVA/DBDMA Nanocomposite Film. TGA was carried out on the fresh and irradiated PVA/DBDMA thin films with the aim to determine the different thermal properties and evaluate the stability of the casted nanocomposite films as well as to assess the impact of the γ-irradiation exposure on the thermal behavior and stability of the PVA/DBDMA film. Thermograms in Figure 17 show that untreated PVA/DBDMA undergoes two principal steps of thermal decomposition. The first occurs at a temperature range of 95−160 °C revealing a weight loss of 4.42% which refers to the removal of moisture and residual solvent,[52] whereas the temperature range at which the second decomposition step occurs is 270−436 °C with a weight loss of 87.15% which represents more significant weight loss due to the degradation of side group (−OH) to give polyene[53] and also the cleavage of (C−C) in the main chain of PVA (leading to carbocation).[54] In addition, these thermal findings showed more enhanced thermal properties of the casted and blended

https://doi.org/10.1021/acsomega.2c03174
ACS Omega 2022, 7, 34002−34011

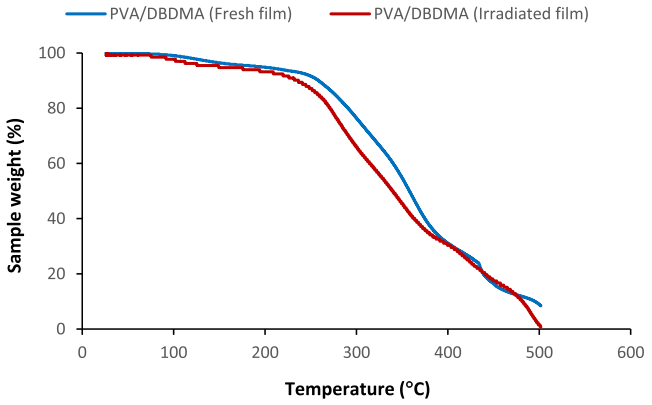

Figure 17. TGA thermograms of fresh and irradiated PVA/DBDMA thin films (dose 210 mR).

PVA/DBDMA film compared to a pure PVA film reported in the literature.[55] We notice that after irradiation the thermal behavior decreased and the decomposition onset after irradiation lowered from 270 to 240 °C. Moreover, the residual weight after degradation of the fresh PVA/DBDMA film (8.43%) was higher than the one observed with the irradiated film (0.12). This confirmed the thermal stability of the prepared PVA/DBDMA film and the effect of the γ-irradiation on its thermal behavior.

3.5.4. SEM Study of the PVP/DBDMA Nanofibers and the PVA/DBDMA Nanocomposite Film. SEM micrograph in Figure 18a shows smooth and regular nanofiber morphology without the appearance of clear nodes or beads. This could be explained by the use of a low flow rate and an appropriate needle-collector distance, allowing enough time for solvent evaporation. Although, by using high flow rates, beads may appear due to the short drying time.[56]

The bead-free fibers revealed a relatively uniform diameter size. Most nanofibers' average diameter ranges from 300 to 400 nm. Moreover, the structure obtained from the above process parameters showed continuous twisted and spaced nanofibers providing a surface porosity which is a required property for various electrospun polymer applications.

This efficient fiber homogeneity in its global morphology was due to the excellent PVP polymer, and appropriate DBDMA selected concentrations allowed suitable viscosity solution to the different applied electrospinning parameters.

After irradiating the nanofiber composite material with the lowest dose of 150 mR (Figure 18b), we noticed the appearance of nodes and beads on the nanofiber structures. The low dose of γ-rays was so low as to cause degradation of the interconnected fibers. By increasing the irradiation dose to 210 mR, nodes and beads became bigger and more apparent (Figures 18c,d). These findings clearly showed the possibility of exploring these materials as sensitive dosimeters with promising application in routine medical diagnostic control.

Morphological SEM analysis of control and irradiated PVA/DBDMA thin films was performed to assess the effect of the increased low-ray doses on the surface morphology of the treated prepared films. Unirradiated PVA/DBDMA film (Figure 19a) presents a smooth and homogeneous appearance with uniform structural integrity and crack-free states. This obtained surface morphology exhibited high compatibility of the two mixed compounds (PVA and DBDMA) and good selection of different parameters for the preparation of the composite film. After low dose γ-irradiation of the PVA/DBDMA nanocomposite films (Figure 19b,c), we remarked the presence of some fluke-like structures accompanied by some globules and surface stripes. These apparently recorded that degradation and morphological changes on the surface morphology of irradiated film composites appeared more vigorous with the increase of the γ-ray applied dose from 210 to 420 mR (Figure 19d). The drastic change in surface morphology of irradiated thin films exhibited high sensitivity of the PVA/DBDMA prepared films and their promising application as low radiation dosimeters for medical diagnostic systems.

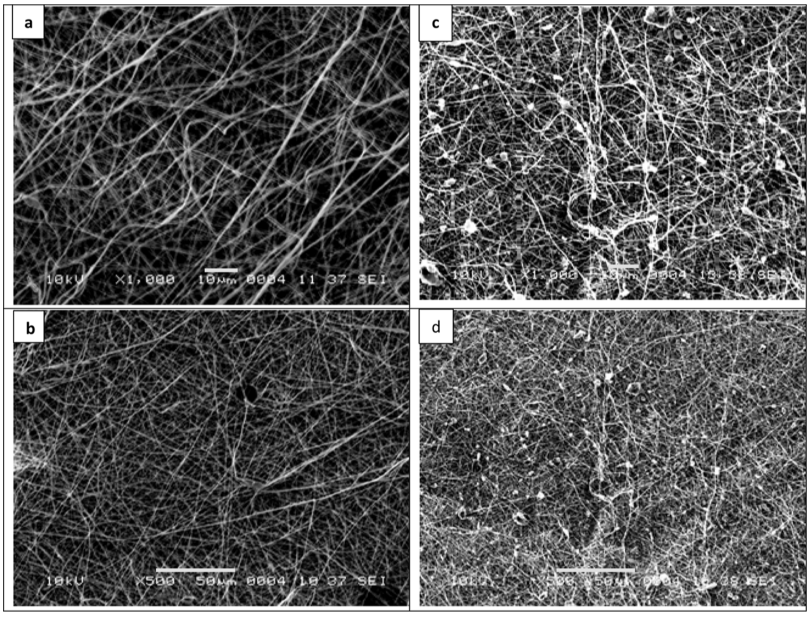

Figure 18. SEM micrographs of PVP/DBDMA nanofibers before irradiation (a) and γ-irradiated samples (b) (dose 150 mR) and (c,d) (at different magnifications, dose 210 mR).

https://doi.org/10.1021/acsomega.2c03174
ACS Omega 2022, 7, 34002−34011

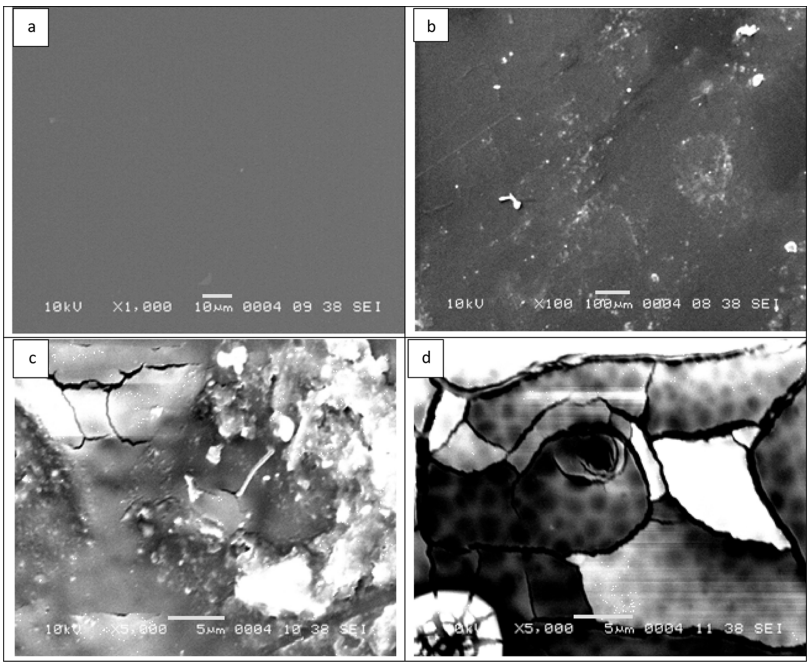

Figure 19. SEM micrographs of the DBDMA/PVA raw thin film (a) and γ-irradiated films (b,c) (dose 210 mR at different magnifications) and (d) (dose 420 mR).

4. CONCLUSIONS

Detection or further quantification of the γ-ray dose to tissues or organs is of great importance for risk estimation, but such doses are arduous to assess directly in most situations. In the current work, we proposed an alternative based on various nanomaterial hosts doped with a new fluorescent dye as effective γ-ray dosimeters. Poor excited-state solvation is indicated by a slight Stokes shift of the studied dye. The valuable colorimetric and optical performances (high optical stability, high fluorescent quantum yield, and short excited-state lifetime value) and the excellent spectral behavior obtained confirmed its ability to be a potent candidate as a sensitive indicator and efficient sensor for dosimetric devices. To these findings, PVP/DBDMA nanofiber materials and PVA/DBDMA thin films were designed, and their preparation parameters were optimized. The dosimetric efficiency of these two nanomaterials after irradiation with different doses of γ-rays was evaluated. Indeed, both prepared materials revealed clear changes in the characteristics of the fluorescence and absorption spectra which became more significant with increased applied doses. Additionally, the thermogravimetric study of PVA thin films via TGA showed good thermal stability of the prepared films and the modification of their thermal proprieties after irradiation. Furthermore, the morphology of the dye-doped PVP and PVA nanomaterials exhibited gradual surface degradation after exposure to increased low dose γ-rays. Therefore, all these findings confirmed the possibility of exploring DBDMA-doped PVP nanofibers and PVA/DBDMA thin films as sensitive dosimeters with promising application in routine medical diagnostic control. Moreover, photostable DBDMA can also be considered a potential laser dye and solar cell collector.

AUTHOR INFORMATION

Corresponding Authors

Sadeq M. Al-Hazmy − *Department of Chemistry, College of Science, Qassim University, Buraidah 51452, Saudi Arabia; Department of Chemistry, College of Science, Sana'a University, Sana'a 1247, Yemen*; Email: s.alhazmi@qu.edu.sa

Yassine EL-Ghoul − *Department of Chemistry, College of Science, Qassim University, Buraidah 51452, Saudi Arabia; Textile Engineering Laboratory, University of Monastir, Monastir 5019, Tunisia*; orcid.org/0000-0001-9520-1793; Email: y.elghoul@qu.edu.sa

Fahad M. Alminderej − *Department of Chemistry, College of Science, Qassim University, Buraidah 51452, Saudi Arabia*; Email: f.alminderej@qu.edu.sa

Authors

Jameelah Al-Harby − *Department of Chemistry, College of Science, Qassim University, Buraidah 51452, Saudi Arabia*

Haja Tar − *Department of Chemistry, College of Science, Qassim University, Buraidah 51452, Saudi Arabia*

Complete contact information is available at: https://pubs.acs.org/10.1021/acsomega.2c03174

Notes

The authors declare no competing financial interest.

ACKNOWLEDGMENTS

The researchers would like to thank the Deanship of Scientific Research, Qassim University for funding the publication of this project.

REFERENCES

(1) Pati, S.; Chatterji, A.; Dash, B. P.; Nelson, B. R.; Sarkar, T.; Shahimi, S.; Edinur, H. A.; Manan, T. S. B. A.; Jena, P.; Mohanta, Y. K.; et al. Structural Characterization and Antioxidant Potential of

https://doi.org/10.1021/acsomega.2c03174
ACS Omega 2022, 7, 34002−34011

Chitosan by γ-Irradiation from the Carapace of Horseshoe Crab. *Polymers* **2020**, *12*, 2361.
(2) Hu, J.; Zhang, M.; He, Y.; Zhang, M.; Shen, R.; Zhang, Y.; Wang, M.; Wu, G. Fabrication and Potential Applications of Highly Durable Superhydrophobic Polyethylene Terephthalate Fabrics Produced by In-Situ Zinc Oxide (ZnO) Nanowires Deposition and Polydimethylsiloxane (PDMS) Packaging. *Polymers* **2020**, *12*, 2333.
(3) Tapia-Guerrero, Y. S.; Del Prado-Audelo, M. L.; Borbolla-Jiménez, F. V.; Gomez, D. M. G.; García-Aguirre, I.; Colín-Castro, C. A.; Morales-González, J. A.; Leyva-Gómez, G.; Magaña, J. J. Effect of UV and Gamma Irradiation Sterilization Processes in the Properties of Different Polymeric Nanoparticles for Biomedical Applications. *Materials* **2020**, *13*, 1090.
(4) Peng, Y. K.; Lui, C. N. P.; Chen, Y. W.; Chou, S. W.; Raine, E.; Chou, P. T.; Yung, K. K. L.; Tsang, S. C. E. Engineering of Single Magnetic Particle Carrier for Living Brain Cell Imaging: A Tunable T1-/T2-/Dual-Modal Contrast Agent for Magnetic Resonance Imaging Application. *Chem. Mater.* **2017**, *29*, 4411−4417.
(5) Li, C. H.; Kuo, T. R.; Su, H. J.; Lai, W. Y.; Yang, P. C.; Chen, J. S.; Wang, D. Y.; Wu, Y. C.; Chen, C. C. Fluorescence-Guided Probes of Aptamer-Targeted Gold Nanoparticles with Computed Tomography Imaging Accesses for in Vivo Tumor Resection. *Sci. Rep.* **2015**, *5*, 15675.
(6) Inaba, Y.; Nakamura, M.; Zuguchi, M.; Chida, K. Development of Novel Real-Time Radiation Systems Using 4-Channel Sensors. *Sensors* **2020**, *20*, 2741.
(7) Vo, P. P.; Doan, H. N.; Kinashi, K.; Sakai, W.; Tsutsumi, N.; Huynh, D. P. X-ray Visualization and Quantification Using Fibrous Color Dosimeter Based on Leuco Dye. *Appl. Sci.* **2020**, *10*, 3798.
(8) Diffey, B. The Early Days of Personal Solar Ultraviolet Dosimetry. *Atmosphere* **2020**, *11*, 125.
(9) Kržanović, N.; Stanković, K.; Živanović, M.; Đaletić, M.; Ciraj-Bjelac, O. Development and testing of a low-cost radiation protection instrument based on an energy compensated Geiger-Müller tube. *Radiat. Phys. Chem.* **2019**, *164*, 108358.
(10) Glais, E.; Massuyeau, F.; Gautier, R. Tuning the oxidation states of dopants: A strategy for the modulation of material photoluminescence properties. *Chem.—Eur. J.* **2020**, *27*, 905−914.
(11) William, J. E. Tutorial on the Role of Cyclopentadienyl Ligands in the Discovery of Molecular Complexes of the Rare-Earth and Actinide Metals in New Oxidation States. *Organometallics* **2016**, *35*, 3088−3100.
(12) Sanyal, B.; Goswami, M.; Shobha, S.; Prakasan, V.; Krishnan, M.; Ghosh, S. K. Thermoluminescence and electron paramagnetic resonance study on rare earth/transition metal doped lithium borate glasses for dosimetry applications. *J. Lumin.* **2019**, *216*, 116725.
(13) Chandler, J. R.; Sholom, S.; McKeever, S. W. S.; Hall, H. L. Thermoluminescence and phototransferred thermoluminescence dosimetry on mobile phone protective touchscreen glass. *J. Appl. Phys.* **2019**, *126*, 074901.
(14) Vo, P. P.; Doan, H. N.; Kinashi, K.; Sakai, W.; Tsutsumi, N. X-ray composite fibrous color dosimeter based on 10,12-pentacosadiynoic acid. *Dyes Pigments* **2021**, *191*, 109356.
(15) AL Zahrany, A.; Rabaeh, K.; Eyadeh, M.; Basfar, A. Dosimetric evaluation of methyl red radiochromic film for radiation processing. *Pigm. Resin Technol.* **2020**, *50*, 157−162.
(16) Loch, C. O.; Eichenberger, M. A.; Togno, M.; Zinsli, S. P.; Egloff, M.; Papa, A.; Ischebeck, R.; Lomax, A. J.; Peier, P.; Safai, S. Characterization of a Low-Cost Plastic Fiber Array Detector for Proton Beam Dosimetry. *Sensors* **2020**, *20*, 5727.
(17) Santos, T.; Ventura, T.; Lopes, M. A review on radiochromic film dosimetry for dose verification in high energy photon beams. *Radiat. Phys. Chem.* **2020**, *179*, 109217.
(18) Alminderej, F. M.; Ammar, C.; El-Ghoul, Y. Functionalization, characterization and microbiological performance of new biocompatible cellulosic dressing grafted chitosan and Suaeda fruticosa polysaccharide extract. *Cellulose* **2021**, *28*, 9821−9835.
(19) EL-Ghoul, Y.; Ammar, C.; Alminderej, F. M.; Shafiquzzaman, M. Design and Evaluation of a New Natural Multi-Layered Biopolymeric Adsorbent System-Based Chitosan/Cellulosic Nonwoven Material for the Biosorption of Industrial Textile Effluents. *Polymers* **2021**, *13*, 322.
(20) Ammar, C.; Alminderej, F. M.; EL-Ghoul, Y.; Jabli, M.; Shafiquzzaman, M. Preparation and Characterization of a New Polymeric Multi-Layered Material Based K-Carrageenan and Alginate for Efficient Bio-Sorption of Methylene Blue Dye. *Polymers* **2021**, *13*, 411.
(21) El-Ghoul, Y. Biological and microbiological performance of new polymer-based chitosan and synthesized aminocyclodextrin finished polypropylene abdominal wall prosthesis biomaterial. *Text. Res. J.* **2020**, *90*, 2690−2702.
(22) Alminderej, M. F.; El-Ghoul, Y. Synthesis and study of a new biopolymer-based chitosan/hematoxylin grafted to cotton wound dressings. *J. Appl. Polym. Sci.* **2019**, *136*, 47625.
(23) Sąsiadek, E.; Jaszczak, M.; Skwarek, J.; Kozicki, M. NBT-Pluronic F-127 Hydrogels Printed on Flat Textiles as UV Radiation Sensors. *Materials* **2021**, *14*, 3435.
(24) Seito, H.; Ichikawa, T.; Hanaya, H.; Sato, Y.; Kaneko, H.; Haruyama, Y.; Watanabe, H.; Kojima, T. Application of clear polymethylmethacrylate dosimeter Radix W to a few MeV electron in radiation processing. *Radiat. Phys. Chem.* **2009**, *78*, 961−965.
(25) Rabaeh, K. A.; Basfar, A. A. A polystyrene film dosimeter containing dithizone dye for high dose applications of gamma-ray source. *Radiat. Phys. Chem.* **2020**, *170*, 108646.
(26) Doyan, A.; Susilawati, S.; Prayogi, S.; Bilad, M. R.; Arif, M. F.; Ismail, N. M. Polymer Film Blend of Polyvinyl Alcohol, Trichloroethylene and Cresol Red for Gamma Radiation Dosimetry. *Polymers* **2021**, *13*, 1866.
(27) Susilawati, S.; Prayogi, S.; Arif, M. F.; Ismail, N. M.; Bilad, M. R.; Asy'ari, M. Optical Properties and Conductivity of PVA−H3PO4 (Polyvinyl Alcohol−Phosphoric Acid) Film Blend Irradiated by γ-Rays. *Polymers* **2021**, *13*, 1065.
(28) Osman, M. I.; Abdalla, D. M.; Elfaki, H. A.; Yagoub, Y. A. K.; Ibrahim Hussein, K.; Eldoma, M. A.; Omer Al-atta, N.; Mohamed Osman Siddig, Y. Effects of additive and gamma irradiation on the structural and optical properties of polyvinyl alcohol doped with silver nitrate. *Glob. Sci. J.* **2021**, *9*, 1780−1792.
(29) Raouafi, A.; Daoudi, M.; Jouini, K.; Charradi, K.; Hamzaoui, A. H.; Blaise, P.; Farah, K.; Hosni, F. Effect of gamma irradiation on the color, structure and morphology of nickel-doped polyvinyl alcohol films: Alternative use as dosimeter or irradiation indicator. *Nucl. Instrum. Methods Phys. Res. Sect. B Beam Interact. Mater. Atoms* **2018**, *425*, 4−10.
(30) Alashrah, S.; El-Ghoul, Y.; Omer, M. A. A. Synthesis and Characterization of a New Nanocomposite Film Based on Polyvinyl Alcohol Polymer and Nitro Blue Tetrazolium Dye as a Low Radiation Dosimeter in Medical Diagnostics Application. *Polymers* **2021**, *13*, 1815.
(31) Horne, J.; McLoughlin, L.; Bridgers, B.; Wujcik, E. K. Recent Developments in Nanofiber-Based Sensors for Disease Detection, Immunosensing, and Monitoring. *Sens. Actuators Rep.* **2020**, *2*, 100005.
(32) Yang, X. P.; Li, L. F.; Yang, D. Z.; Nie, J.; Ma, G. P. Electrospun Core−Shell Fibrous 2D Scaffold with Biocompatible Poly(Glycerol Sebacate) and Poly-L-Lactic Acid for Wound Healing. *Adv. Fiber Mater.* **2020**, *2*, 105−117.
(33) EL-Ghoul, Y.; Alminderej, F. M.; Alsubaie, F. M.; Alrasheed, R.; Almousa, N. H. Recent Advances in Functional Polymer Materials for Energy, Water, and Biomedical Applications: A Review. *Polymers* **2021**, *13*, 4327.
(34) Lv, D.; Zhu, M. M.; Jiang, Z. C.; Jiang, S. H.; Zhang, Q. L.; Xiong, R. H.; Huang, C. B. Green Electrospun Nanofibers and Their Application in Air Filtration. *Macromol. Mater. Eng.* **2018**, *303*, 1800336.
(35) Nagiah, N.; Murdock, C. J.; Bhattacharjee, M.; Nair, L.; Laurencin, C. T. Development of Tripolymeric Triaxial Electrospun Fibrous Matrices for Dual Drug Delivery Applications. *Sci. Rep.* **2020**, *10*, 609.

https://doi.org/10.1021/acsomega.2c03174
ACS Omega 2022, 7, 34002−34011

(36) Kubota, Y.; Tsuzuki, T.; Funabiki, K.; Ebihara, M.; Matsui, M. Synthesis and fluorescence properties of a pyridomethene− BF2 complex. *Org. Lett.* **2010**, *12*, 4010−4013.
(37) El-Daly, S. A.; Al-Hazmy, S. M.; Ebeid, E. M.; Bhasikuttan, A. C.; Palit, D. K.; Sapre, A. V.; Mittal, J. P. Spectral, acid− base, and laser characteristics of 1, 4-Bis [*β*-(2-quinolyl) vinyl] benzene (BQVB). *J. Phys. Chem.* **1996**, *100*, 9732−9737.
(38) Coe, B. J.; Harris, J. A.; Asselberghs, I.; Clays, K.; Olbrechts, G.; Persoons, A.; Hupp, J. T.; Johnson, R. C.; Coles, S. J.; Hursthouse, M. B.; Nakatani, K. Quadratic Nonlinear Optical Properties of N-Aryl Stilbazolium Dyes. *Adv. Funct. Mat.* **2002**, *12*, 110−116.
(39) Mnasri, A.; Mejri, A.; Al-Hazmy, S. M.; Arfaoui, Y.; Özdemir, I.; Gürbüz, N.; Hamdi, N. Silver−N-heterocyclic carbene complexes-catalyzed multicomponent reactions: Synthesis, spectroscopic characterization, density functional theory calculations, and antibacterial study. *Arch. Pharmazie* **2021**, *354*, 2100111.
(40) Alashrah, S.; El-Ghoul, Y.; Almutairi, F. M.; Omer, M. A. A. Development, Characterization and Valuable Use of Novel Dosimeter Film Based on PVA Polymer Doped Nitro Blue Tetrazolium Dye and AgNO3 for the Accurate Detection of Low X-ray Doses. *Polymers* **2021**, *13*, 3140.
(41) Qin, W.; Baruah, M.; Stefan, A.; Van der Auweraer, M.; Boens, N. Photophysical properties of BODIPY-derived hydroxyaryl fluorescent pH probes in solution. *Chem. Phys. Chem.* **2005**, *6*, 2343−2351.
(42) Bouit, P. A.; Kamada, K.; Feneyrou, P.; Berginc, G.; Toupet, L.; Maury, O.; Andraud, C. Two-photon absorption-related properties of functionalized BODIPY dyes in the infrared range up to telecommunication wavelengths. *Adv. Mat.* **2009**, *21*, 1151−1154.
(43) Ulrich, G.; Ziessel, R.; Harriman, A. The chemistry of fluorescent bodipy dyes: versatility unsurpassed. *Angew. Chem., Int. Ed.* **2008**, *47*, 1184−1201.
(44) Zhang, D.; Wang, Y.; Xiao, Y.; Qian, S.; Qian, X. Long-wavelength boradiazaindacene derivatives with two-photon absorption activity and strong emission: versatile candidates for biological imaging applications. *Tetrahedron* **2009**, *65*, 8099−8103.
(45) Schäfer, F. P. 1. Principles of dye laser operation. *Dye lasers* **1973**, 1−89.
(46) Fork, R. L.; Greene, B. I.; Shank, C. V. Generation of optical pulses shorter than 0.1 psec by colliding pulse mode locking. *App. Phys. Let.* **1981**, *38*, 671−672.
(47) Sadeghi, S.; Bahmani Jalali, H. B.; Srivastava, S. B.; Melikov, R.; Baylam, I.; Sennaroglu, A.; Nizamoglu, S. High-performance, large-area, and ecofriendly luminescent solar concentrators using copper-doped InP quantum dots. *Iscience* **2020**, *23*, 101272.
(48) Mishra, Y. N.; Yoganantham, A.; Koegl, M.; Zigan, L. Investigation of five organic dyes in ethanol and butanol for two-color laser-induced fluorescence ratio thermometry. *Optics* **2020**, *1*, 1−17.
(49) Fu, G. L.; Pan, H.; Zhao, Y. H.; Zhao, C. H. Solid-state emissive triarylborane-based BODIPY dyes: Photophysical properties and fluorescent sensing for fluoride and cyanide ions. *Org. Biomol. Chem.* **2011**, *9*, 8141−8146.
(50) Zhao, C. H.; Sakuda, E.; Wakamiya, A.; Yamaguchi, S. Highly Emissive Diborylphenylene-Containing Bis (phenylethynyl) benzenes: Structure−Photophysical Property Correlations and Fluoride Ion Sensing. *Chem.—Eur. J.* **2009**, *15*, 10603−10612.
(51) Ghorai, S.; Laskin, A.; Tivanski, A. V. Spectroscopic evidence of keto− enol tautomerism in deliquesced malonic acid particles. *J. Phys. Chem. A* **2011**, *115*, 4373−4380.
(52) Awada, H.; Daneault, C. Chremical modification of poly (vinyl alcohol) in water. *Appl. Sci.* **2015**, *5*, 840−850.
(53) Negim, E. S. M.; Rakhmetullayeva, R. K.; Yeligbayeva, G. Zh.; Urkimbaeva, P. I.; Primzharova, S. T.; Kaldybekov, D. B.; Khatib, J. M.; Mun, G. A.; Craig, W. Improving biodegradability of poly vinyl alcohol/starch blend films for packaging applications. *Int. J. Basic Appl. Sci.* **2014**, *13*, 263−273.
(54) Duraikkan, V.; Sultan, A. B.; Nallaperumal, N.; et al. Structural, thermal and electrical properties of polyvinyl alcohol/poly(vinyl pyrrolidone)−sodium nitrate solid polymer blend electrolyte. *Ionics* **2018**, *24*, 139−151.
(55) Betti, N. A. Thermogravimetric analysis on PVA/PVP blend under air atmosphere. *Eng. Technol. J.* **2016**, *34*, 2433−2441.
(56) Athira, K. S.; Chatterjee, K. Fabrication of poly (Caprolactone) nanofibers by electrospinning. *J Polym. Biopolym. Phys. Chem.* **2014**, *2*, 62−66.

https://doi.org/10.1021/acsomega.2c03174
ACS Omega 2022, 7, 34002−34011